JOURNAL OF PROPULSION AND POWER
Vol. 12, No. 1, January–February 1996

Wall Surface Leakage Effects on Magnetohydrodynamic Power Generator Performance

Carlson C. P. Pian* and Edwin W. Schmitt†
Textron Defense Systems, Everett, Massachusetts 02149

Internal surface-leakage effects on magnetohydrodynamic power generator performance were studied using a combined experimental and analytical approach. A method to determine the wall resistance and slag layer conductivity distributions from seed shutoff test data is introduced. These measured resistance values were then utilized in generator performance analyses. Calculated generator variables were compared with measured data to verify the modeling approach. Finally, these calculated results were used to investigate the distribution of internal leakage currents as a function of generator size, generator operating conditions, and iron oxide injection rates. An advantage of this analysis methodology is the ability to differentiate wall leakage from apparent leakage effects in the measured test data.

Nomenclature

A	=	channel cross-sectional area, m^2
H	=	channel height, m
H'	=	height of iron oxide wake, m
I	=	current, A
L	=	streamwise distance over which voltage differences were measured, m
P	=	channel cross-sectional perimeter, m
p	=	electrode pitch, m
R	=	electrical resistance, Ω/gap
s	=	slag layer thickness, m
W	=	channel width, m
X, X_a	=	streamwise distance, m
ΔV	=	measured voltage differential, V
σ	=	electrical conductivity, mho/m
ϕ	=	combustion equivalence ratio

Subscripts

asg	=	anode wall slag layer
csg	=	cathode wall slag layer
gap	=	insulator gap
i	=	iron-rich slag layer
plasma	=	plasma value
ps	=	power supply value
sg, slag	=	mean slag layer value
swsg	=	sidewall slag layer

Introduction

THE internal surfaces of coal-fired magnetohydrodynamic (MHD) power generator channels are coated with a layer of molten slag. The slag coating reduces heat loss to the channel walls, but can also increase the internal current leakage of the generator. The purpose of this study is to gain a better understanding of wall leakage and how it affects the performance of MHD generators. This task is not straightforward because internal leakage currents cannot be directly measured during power tests, and because it is difficult to differentiate actual wall leakage from apparent leakage in the test data.

Received Sept. 23, 1994; revision received July 11, 1995; accepted for publication July 24, 1995.

*Director, Commercial MHD Component Development; currently at Diagnostic Instrumentation and Analysis Laboratory, Mississippi State University, Mississippi State, MS 39762. Senior Member AIAA.

†Senior Engineer, Energy Technology Office. Member AIAA.

Iron oxide injection further complicates efforts to determine the amount of internal leakage. Iron oxide is sometimes added to the cathode wall slag layer during the operation of MHD generators in order to prevent slag-induced voltage nonuniformities. This voltage nonuniformity phenomenon has been extensively reported.[1,2] Voltage nonuniformities arise when groups of adjacent cathodes are shorted by polarized slag. As a result, the generator Hall voltage is sustained by only a few nonshorted intercathode gaps. The voltages across these open cathode gaps are substantially higher than when no slag shorting occurs. An example of cathode voltage nonuniformities, measured during generator tests at the U.S. Department of Energy's MHD Component Development and Integration Facility (CDIF), is shown in the top plot of Fig. 1. The generator's Hall voltage is sustained along the cathode wall by approximately 60 insulator gaps (out of 280 available intercathode gaps). The remaining gaps are shorted by the polarized slag. The appearance of these voltage nonuniformities can reduce both performance and lifetime.

Polarization can be alleviated by modifying the slag layer chemistry with the addition of iron oxide.[2] A typical intercathode voltage distribution, measured during a generator test with iron oxide injection, is shown in the bottom plot of Fig. 1. In

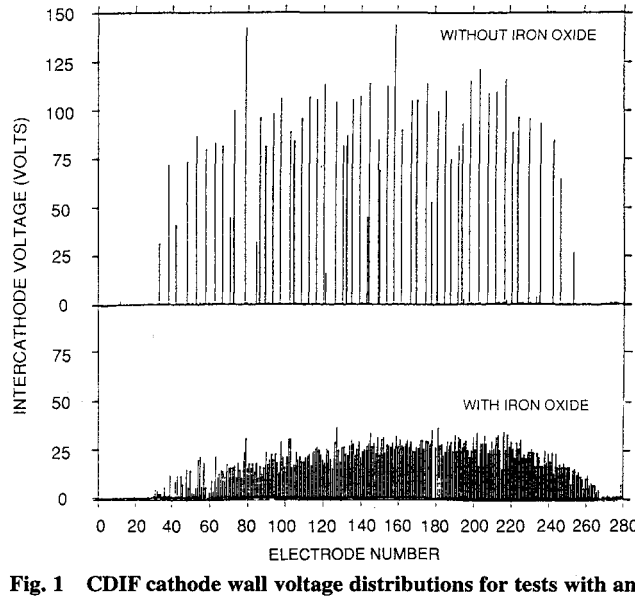

Fig. 1 CDIF cathode wall voltage distributions for tests with and without iron oxide addition.

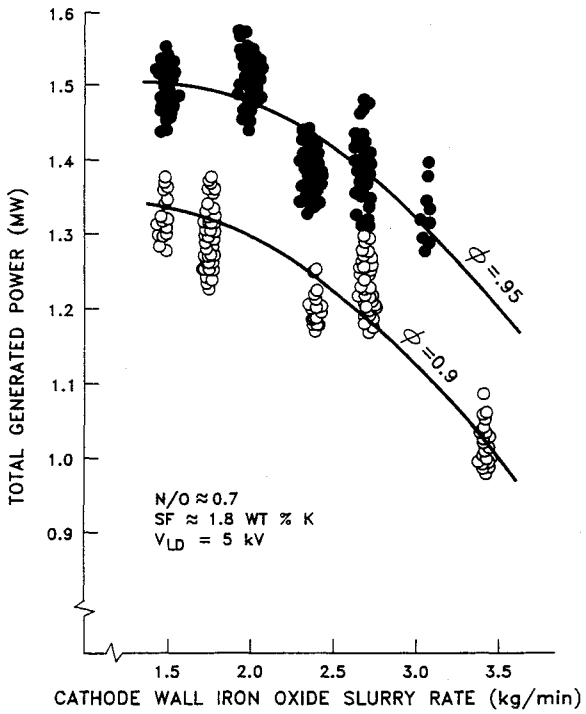

Fig. 2 Variations of generator power output at different iron oxide slurry rates during test 90-DIAG-13 at the CDIF. ϕ less than one denotes fuel rich conditions. Circles represent data measurements taken at 5-s intervals.

this case, the slag-induced shorting is eliminated and the generator axial voltage is distributed among all of the insulator gaps, with a typical intercathode voltage of less than 35 V.

Although iron oxide can be beneficial in eliminating axial shorting due to slag polarization, it can itself contribute to increased surface leakage. This can become a problem, especially if the iron oxide is injected improperly or if too much is added. The decrease in measured power output for increasing iron oxide slurry rates is shown in Fig. 2. Measurements (for two different combustion equivalence ratios) showed power output reductions of approximately 400 kW when the iron oxide slurry rate was increased from 1.4 to 3.6 kg/min. The decreased performance is caused primarily by increased transverse and axial current leakages in the iron-rich slag layers.

One of the goals of this investigation was to better understand the wall leakage due to iron oxide injection. The distributions of internal wall resistance under actual generator operating conditions can be extremely difficult to ascertain. Iron oxide slurry typically is injected onto the cathode wall through ports situated upstream of the generator inlet nozzle. The resulting iron oxide wake spreads along the cathode wall and up the two sidewalls. The concentration of iron oxide in the slag layers also decreases with increasing axial distance. The axial variations of the generator wall resistance, as well as the electrical conductivity of the iron-rich slag layers, are dependent on many factors. These factors include the rate of iron oxide slurry injection, location and method of slurry injection, channel length, and slag carryover rate.

Excessive potassium seed concentration in the channel wall slag layers also can cause increased internal leakage. High seed concentration may result from poor upstream seed injection or may be caused by the runoff of seed-contaminated slag from the combustor. Generator voltages and currents are reduced as a result of this seed-induced wall shorting.[3]

Difficulties and weaknesses with previous methods of estimating internal currents, based upon posttest data analysis, are described later. These methods usually resulted in modeling inconsistencies or in very large, and sometimes unrealistic, values of leakage currents.

A common approach used previously to determine leakage currents was to carry out MHD generator performance analyses using estimated values of wall resistances determined from fundamental slag studies. The distributions of the wall leakage currents were then calculated from a computer model.[4] The weakness with this approach is that the actual wall resistance distributions are frequently not known. Slag deposits on the channel walls typically have large variations in composition, temperature, and uniformity. Also, slag layer electrical conductivities can have substantial amounts of axial variation due to iron oxide injection and seed contamination of the slag.

A variation on the previous approach for estimating wall currents was used in Refs. 5 and 6. Here, computer analyses simulated the conditions representative of the test data. The magnitudes of the leakage current in the analyses were parametrically varied until a match was obtained between the calculated and measured generator electrical outputs. The leakage current was then defined as the gross axial current required to obtain this data match. The problem with this approach, when applied to generator test results, is that often very large values of leakage currents are inferred. In Ref. 5, assumed axial leakage currents in excess of 140 A were required to obtain data matches with the CDIF generator test data. It is very unlikely that this generator could have generated the measured power outputs if such large axial currents actually existed within the channel at the particular test operating conditions, especially since these tests were carried out without iron oxide addition. Because this approach infers the leakage current value from the difference between the model results and the measured results, any factor that affects the generator performance, but that has not been explicitly included in the particular model formulation, is also interpreted as a leakage loss. For example, if the mixing of oxygen injection jets in the combustor second-stage duct was incomplete during a particular test, and the resulting test data are analyzed with a generator model that assumed uniform plasma flow, then the power shortfall due to poor flow mixing could be interpreted as wall leakage effects. Other possible contributions to this apparent leakage include finite electrode segmentation effects, boundary-layer effects, and flow nonuniformities.

Reference 7 describes another approach to determine the leakage current in which special models are developed to solve for the wall resistance (and another variable, usually the plasma conductivity). The models required measured electrical variables as inputs (usually the measured Hall voltage and averaged value of the electrode currents), while values for other generator variables are assumed (such as boundary-layer voltage drops, Hall parameter, and flow velocity). References 8 and 9 report on similar model formulations that infer values of leakage currents indirectly from measured test data. As in other indirect methods, these models cannot differentiate real wall leakage from apparent leakage. In fact, the effects of plasma nonuniformities and leakage current losses are not only difficult to separate in these models, but their effects are interchangeable.[6]

In this article we introduce an experimental approach using seed shutoff test data to determine wall resistance and slag layer conductivity distributions under actual generator operating conditions. These measured wall resistances are then used in generator performance analyses. An advantage of this approach is that the effects of iron oxide addition and seed-induced wall shorting are taken into account as part of the data analysis. The results of computer analyses are used to quantify how the overall generator performance is diminished by wall leakage currents and by iron oxide addition. These results are also used to estimate the magnitudes of leakage currents and to determine how they are distributed among the four walls.

Approach

The overall approach taken in this study is as follows. First, MHD generator data from oil-fired, ash-injection combustor (AIC) tests were used for exploratory wall leakage studies. Ash-injection is used to simulate coal-fired generator operating conditions. The AIC generator tests were carried out during 1982 and 1983 at the CDIF, and during 1989 and 1990 in a generator test facility (Mk-VII MHD facility) situated in Everett, MA. The AIC test data are ideal for these exploratory studies. They tended to be more steady and more repeatable than coal-fired test data. Also, AIC test results are available over a much wider range of generator operating parameters (i.e., generator loading, iron oxide injection rate, oxidant N/O ratio, combustion stoichiometry, magnetic field strength, and slag-carryover rate). After confirming our leakage modeling approach with these AIC data, we proceeded to analyze the coal-fired MHD generator test data.[3]

Generator wall resistance and slag layer conductivity distributions are determined from seed shutoff tests. Resistance values were measured for a variety of wall conditions, including bare walls, walls with seeded slag, and walls with iron oxide addition. These measured resistance profiles are then used in our calculations to predict the generator performance under power generating conditions. Here, we make the assumption that the wall resistance profiles measured under seed shutoff conditions (nonpower generating conditions) are similar to the resistance distributions under the corresponding power generating conditions. To validate this approach, calculations were carried out and compared with a wide range of available generator test data including 1) AIC vs coal-fired tests, 2) Mk-VII (20-MW_t) vs CDIF (50-MW_t) tests, 3) Faraday vs diagonally loaded generator tests, 4) generator tests with and without iron oxide addition, 5) tests with various oxidant N/O ratios, and 6) tests with different values of combustor equivalence ratio. The excellent agreements obtained in all of these data comparisons confirm our wall leakage assumption. The results of the analyses were then used to determine generator leakage current distributions as a function of generator size, generator loading, and iron oxide injection rate.

Results

Results from the reduction of AIC generator test measurements and data analyses are reported herein. Wall resistance profiles were first obtained from the Mk-VII seed shutoff tests. These resistance values were then used in performance calculations for Mk-VII generator power tests. Results for the CDIF MHD generator test data (AIC and coal-fired) are reported in Ref. 3.

Mk-VII Seed Shutoff Results

The seed shutoff tests were carried out in the Mk-VII MHD facility during 1989 and 1990 in order to ascertain resistance values of the generator walls.[10] These data have been re-examined and additional information has been extracted concerning the nature of surface leakage currents during iron oxide injection. These new data interpretations are described next.

These seed shutoff tests were carried out for a variety of wall surface conditions, including bare walls, walls covered with potassium-seeded slag, and walls with iron-rich, potassium-seeded slag. The test procedure involved the controlled termination of seed injection under a constant externally applied axial voltage of 400 V. A schematic diagram of this configuration is shown in Fig. 3, which also shows the directional paths that the currents will take. The measured power supply current during a typical seed shutoff period is shown in Fig. 4. Before the seed was terminated, a power supply current of about 32 A was measured for this particular test. This current represents the sum of the currents flowing through the plasma and the slag layers, as shown by the sketch in Fig. 3. The

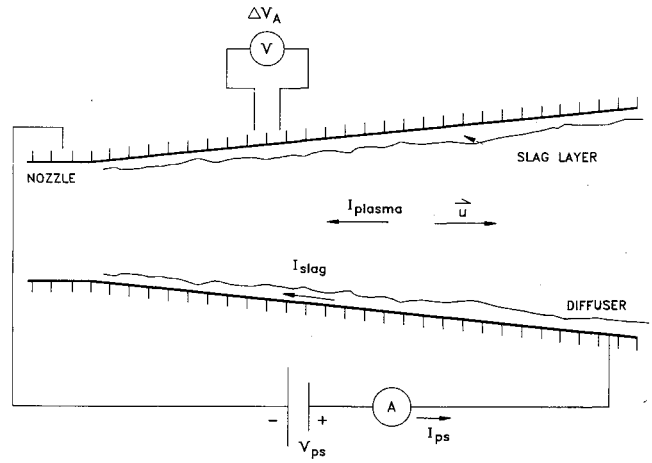

Fig. 3 Setup for seed shutoff tests and plasma conductivity measurements.

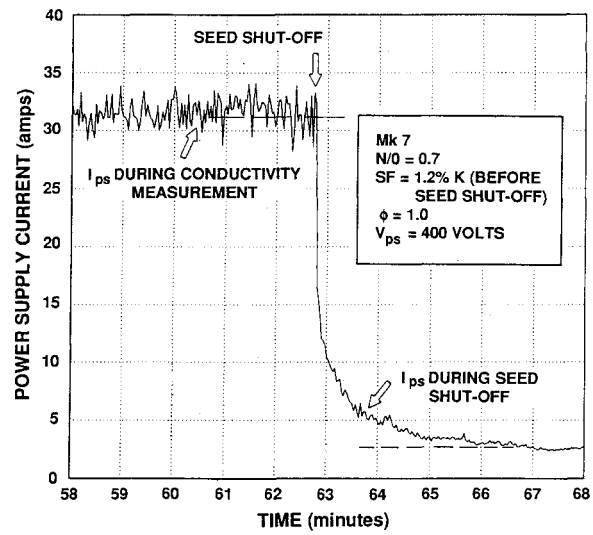

Fig. 4 Variations in the measured power supply current during a typical Mk-VII seed shutoff test.

power supply current drops suddenly just after the seed valve is closed, indicating a loss of plasma conductivity. After this very rapid decay, there exists a transition period, lasting between 1–3 min, during which the out-gassing of the seed from the slag layer to the gas will continue to contribute significantly to the bulk plasma conductivity and to the measured power supply current. This is indicated by the elbow in the power supply current vs time curve. As discussed in detail later, after this transition period the plasma conductivity is reduced to a level where almost all of the measured power supply current (about 3 A for the particular test of Fig. 4) represents the current flowing only through the slag layer leakage paths. This established a lower bound on the estimate of seeded slag layer resistance. A long time after seed shutoff, the potassium seed in the slag would eventually be depleted and the power supply current would decay asymptotically to approximately 1.5 A, the value of wall leakage current for the unseeded slag used in this test.

Experimental observations support the proposition that the measured power supply current near the end of the elbow period in Fig. 4 represented mostly current flowing through the seeded slag layer leakage paths, with very little contribution to the total current from the plasma region. It has been observed that the characteristic times for plasma conductivity decay after seed shutoff are of the orders of a few minutes, while

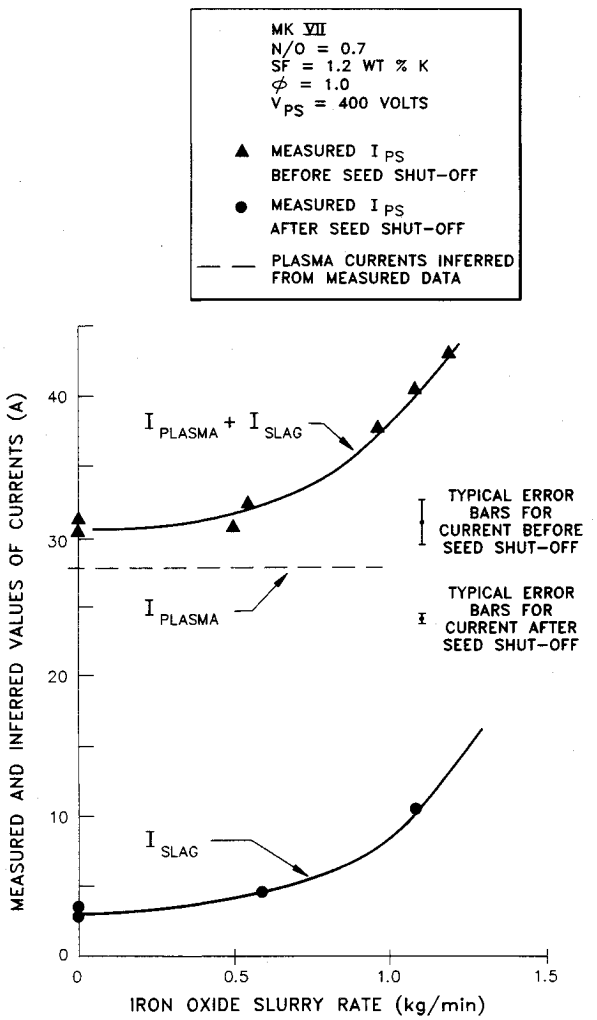

Fig. 5 Measured and inferred values of currents for different iron oxide slurry rates.

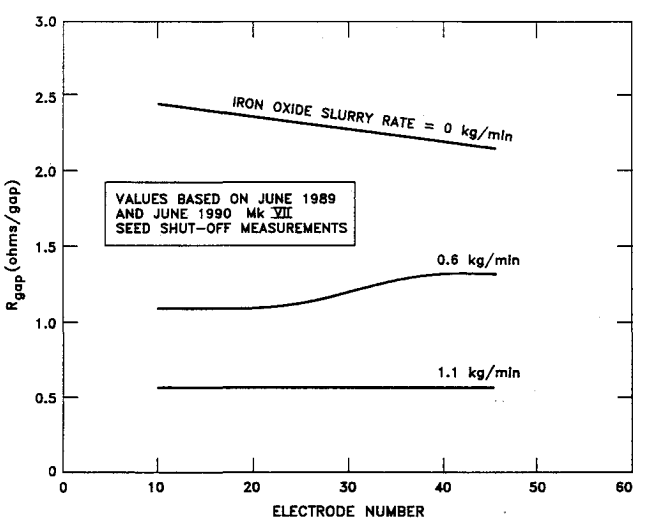

Fig. 6 Axial gap resistance distributions from the Mk-VII seed shutoff tests.

several tens of minutes are required before out-gassing of seed alters the slag layer resistance.[3]

The bulk plasma conductivity decay times can be ascertained from results of seed termination tests where contributions to gas conductivity by surface evaporation are minimized, such as tests using bare wall channels or using liquid seed. The former tests, conducted without ash injection, resulted in little surface seeding. Measured power supply currents typically drop to less than 1 A a few minutes after seed termination. In the latter tests, the potassium seed is injected into the channel as an aqueous solution. Atomization of liquid seed is very efficient, resulting in very low seed entrainment into the slag layers. Again, the measured power supply currents drop quickly to about 1.5 A. From these results, one can conclude that plasma conductivity is insignificant approximately 3 to 5 min after seed termination for the test conditions of Fig. 4.

The times required for the seed to out-gas from the slag layer can be determined by monitoring the time evolution of the measured interelectrode voltage after seed termination. The local slag resistances change very slowly, requiring times in excess of 30–45 min after seed termination to reach steady state. In situations where high seed concentrations in the slag layers are known a priori, such as in the inlet regions of coal-fired MHD channels and at channel locations just downstream of the seed injectors, very low interelectrode voltages (as well as local shorts) were measured.[3] Typically, these low slag resistance regions would persist for 20–30 min after seed termination. The large differences between the time scales for plasma seed depletion and for the seed to out-gas from the slag confirms that the conditions of the slag layers at about 3–5 min after seed shutoff are representative of those conditions before seed termination and during power generation.

The values of power supply currents I_{ps} measured before and after seed shutoff are shown in Fig. 5 for various iron oxide injection rates. The topmost curve is the measured I_{ps} before the seed shutoff, which represents the sum of internal currents flowing in the plasma and through the slag layers. The bottom curve in the figure is the I_{ps} values measured at about 3 min after seed shutoff, which represents the magnitude of the leakage current through the seeded slag layer I_{slag}. The third curve in this figure represents the current flowing through the plasma I_{plasma}. The magnitude of this current is the difference between the measured I_{ps} before and after the seed shutoff.

Figure 5 clearly shows the increased surface leakage effects when iron oxide is introduced. When iron oxide is not used, the contribution of the wall/slag layer leakage paths to the total I_{ps} is negligible; almost all of the measured I_{ps} flows through the plasma. This implies that the effective wall resistance is considerably larger than the plasma bulk resistance. However, the effective wall resistances are reduced substantially at higher iron oxide slurry rates, with wall resistance values approaching that of the bulk plasma resistance. For example, at the 1.2 kg/min iron oxide injection rate test condition, over a third of the total measured I_{ps} flows through the channel by way of slag layer leakage paths.

The results shown in Fig. 5 have implications for the interpretation of the plasma conductivity measurements that are routinely taken as part of the generator tests at the CDIF and other MHD facilities. The procedure for determining plasma conductivity is described in Appendix A. I_{ps} measurements are typically used to determine the distributions of the plasma conductivity. This is acceptable without iron oxide injection, since the measured I_{ps} is, in effect, the current flowing through the plasma. However, the difference between the measured I_{ps} and I_{plasma} cannot be ignored when iron oxide is used, or gross errors can result in the inferred gas conductivity values. For example, a 43% overprediction of the plasma conductivity would occur for the 1.2 kg/min iron oxide injection case if one uses the measured I_{ps} (40 A) instead of I_{plasma} (28 A).

The wall resistance distributions for the Mk-VII channel at various iron oxide slurry rates are shown in Fig. 6. The resistance values R_{gap} in this figure are defined as an equivalent four-wall resistance, taking into account the resistances of the anode, cathode, and both sidewalls. The approach for determining these R_{gap} from seed shutoff test measurements is described in Appendix B. The wall resistance for channel surfaces covered with potassium-seeded slag vary between 2–2.5

Ω per insulator gap (or ohms per electrode pitch). The streamwise variations of R_{gap} suggest that the wall resistance varies inversely with the channel cross-sectional perimeter (i.e., slag layer conductivity for seeded slag is nearly constant with streamwise distance). When 0.6 kg/min of iron oxide slurry is introduced onto the cathode wall, the equivalent four-wall resistance is lowered to the range of 1–1.5 Ω/gap. The shape of the R_{gap} distribution indicates that shorting effects of the iron oxide wake occur predominately in the front half of the channel at the 0.6 kg/min slurry injection rate. When the iron oxide injection rate is increased to 1.1 kg/min, the magnitude of R_{gap} profile is further reduced by a factor of 2.

The mean electrical conductivities for the different slag layers can also be estimated from the seed shutoff test data. The spatial variations of σ_{slag} for potassium-seeded slag layers and iron-rich (and seeded) slag layers in the Mk-VII generator channel are compared in Fig. 7, assuming a 1-mm thick slag layer thickness. The methods for determining these slag conductivity values, as well as the simplifying assumptions, are included in Appendix B. The σ_{slag} values labeled without iron oxide in Fig. 7 are applicable to seeded slag layers coating any of the channel walls (anode, cathode, or sidewalls) when iron oxide is not used; as well as for those wall regions not affected by the iron oxide wake (e.g., the anode wall and upper portions of the sidewalls) when iron oxide is injected onto the cathode wall. The values of slag conductivities denoted by 0.6 and 1.1 kg/min iron oxide rates apply to iron-rich slag layers on the cathode wall and over portions of the sidewalls that are immersed in the spreading iron oxide wake.

The range of slag conductivity values at a given axial location is due to several reasons. Some of the variations in σ_{slag} are due to test-to-test differences in the measured data. The Mk-VII seed shutoff tests were conducted over a two-year span during which the channel was reconstructed several times. Additionally, the iron oxide wake patterns measured during posttest inspections, which were used to establish the spread in the iron oxide up the sidewalls, varied from test to test. The iron oxide wake typically grows linearly with streamwise distance and extends about one quarter to halfway up the sidewalls (depending upon injection and wall conditions) by the end of the 1-m Mk-VII channel. Variations in the values of the iron-rich σ_{slag} shown in Fig. 7 correspond to these observed differences in the spreading of the iron oxide wakes.

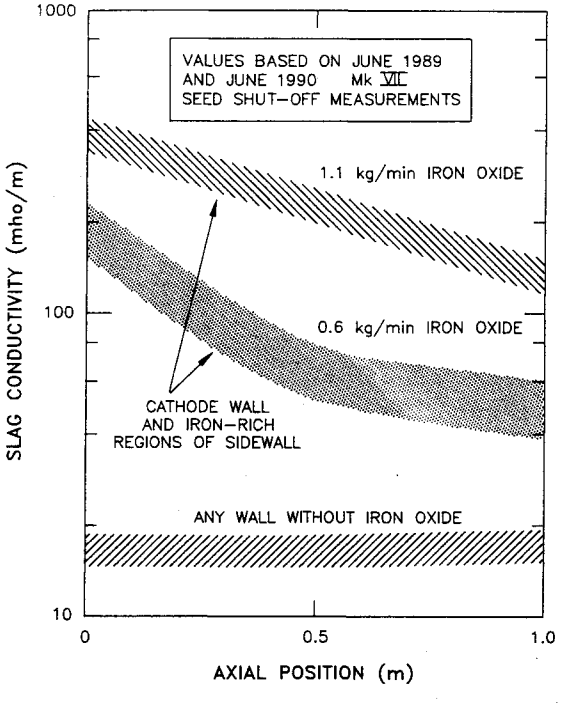

Fig. 7 Typical mean values of slag layer electrical conductivity in the Mk-VII channel. Assumes 1-mm slag layer thickness.

Results of Fig. 7 show that the cathode wall slag conductivity can be substantially increased as a result of iron oxide injection. When approximately 0.6 kg/min of iron oxide slurry is added, the cathode wall σ_{slag} in the inlet region of the Mk-VII channel can be a factor of 10 higher than that of the anode slag layer. This difference between the cathode and anode slag conductivities decreases with axial distance as a result of the spreading of the wakes and the subsequent decrease in the iron concentration in the cathode wall slag layer. By the exit of the Mk-VII channel, the cathode slag layer conductivity is about three times as high as that of the anode wall. When approximately 1.1 kg/min of iron oxide is added, the cathode slag conductivities are at least 10–20 times higher than that of the anode slag layer over the length of the channel. The effects of these elevated cathode wall slag layer leakages on the generator performance are discussed in the next section.

Mk-VII Power Test Data Analyses

The Mk-VII power generation tests were originally carried out during 1989 and 1990 as part of a series of MHD experiments supporting the design and operation of the generator for the integrated topping cycle (ITC) MHD project.[10] Parametric variations in cathode wall iron oxide injection rate and generator loading were carried out during these MHD generator tests. The supersonic test channel was 1 m long, having 56 segmented electrode pairs. The generator was configured with current control devices in its external diagonal electrical connections that spanned eight overlapping electrodes (the angle between the diagonal and vertical planes was approximately 34 deg). Test conditions and channel geometry are listed in Table 1. Measurements of electrical power output, electrode currents, interelectrode, and Faraday voltages were taken at the various generator operating conditions.

The Mk-VII test results have been compared to the posttest analysis of the generator using an MHD generator performance prediction computer code.[11,12] This generator model is based on a coupled core flow-integral boundary-layer formulation. Joule dissipation effects within the electrode boundary layers and the possibility of velocity overshoots in the sidewall boundary layers are included in the analyses of the turbulent boundary layers. The channel geometry, magnetic field intensity, and diagonal electrical connections are prescribed in the analyses. The mass flux, oxidant N/O ratio, combustion equivalence ratio, seed fraction, and combustor/nozzle heat loss measured experimentally are inputs. Finally, the mean values of the slag layer electrical conductivities and slag layer thickness from Fig. 7 are used in the generator analyses in order to provide the proper wall resistances at the various cathode wall iron oxide injection rates. This wall leakage modeling is dif-

Table 1 Operating ranges of 1989–1990 Mk-VII generator tests

Total mass flow rate, 2.0 kg/s
Oxidant N/O ratio, 0.7–0.8
Seed fraction (% wt. potassium), 0.95–1.3
Oxygen stoichiometry, 1.0
Equivalent ash carryover rate, 30%
Coal ash type, western U.S. coal
Iron oxide slurry rate, 0–1.2 kg/min
Diagonal load resistance, short circuit, 5, 15, 20, 30, 80, and open circuit, Ω
Magnetic field intensity, 2.5 T
Channel length, 1.0 m
Channel height
Inlet, 0.15 m
Outlet, 0.18 m
Channel width
Inlet, 0.07 m
Outlet, 0.12 m

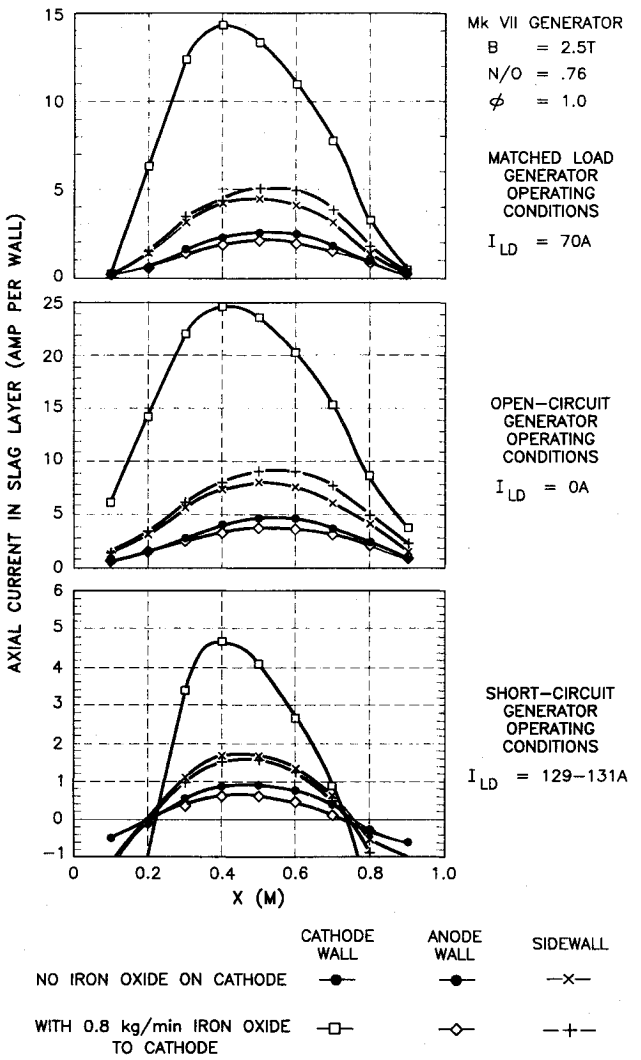

Fig. 8 Spatial distributions of axial wall currents for different rates of cathode wall iron oxide addition.

ferent from that used in earlier generator calculations.[11] In previous analyses, the calculated results are obtained from an iterative solution scheme in which the values of the wall resistance were varied during each of the iterative steps, until the calculated results agreed with the measured values. Typically, the shapes of the axial profile are assumed and the magnitudes of the wall resistance are varied during the iterative steps. By contrast, in the present analyses, the only required assumption is that the channel wall resistances during power generation tests are similar to that measured during corresponding seed shutoff tests.

The calculated generator performances were compared with measured results. Good agreement is obtained both in the overall generator performance, such as generator operating load lines at various cathode iron oxide addition rates, and in local generator characteristics, such as streamwise variations of interanode voltage, Faraday voltage, and electrode current.[3] The excellent agreements in all of these data comparisons confirm our wall leakage modeling approach.

The analysis results are also used to estimate the magnitudes of the internal leakage currents and to determine how they are distributed on the various channel walls. As mentioned previously, none of these internal leakage characteristics can be directly measured during the conduct of MHD generator power tests. Figure 8 shows the axial distributions of the calculated leakage currents at the matched load, open-circuit, and short-circuit operating conditions of the generator. Results for 0 and 0.8 kg/min slurry injection rates are presented to show the changes in leakage current distribution due to cathode iron oxide addition. In the absence of iron oxide injection, leakages on the anode and cathode walls were similar. The sidewall axial currents were larger than those on the two electrode walls because the height of the Mk-VII sidewalls is larger than the width of the electrode walls. The channel cross-sectional aspect ratio *H/W* varied from 2.28 near the inlet to 1.53 at the exit. When iron oxide is injected, most of the increase in the surface current leakage occurred on the cathode wall. Compared to no iron oxide addition, the cathode wall leakage current at the 0.8 kg/min injection rate was about five times larger. The values of axial currents on the sidewall increased slightly towards the rear half of the channel as a result of the spreading iron oxide wake. The decrease of the anode wall current resulted from the reduced generator Hall field when iron oxide is introduced. The maximum value of the total leakage current (occurring near midchannel location) was about 15 A without iron oxide addition. This peak current value increased to over 26 A at the 0.8 kg/min slurry injection rate.

The magnitudes and directions of the axial plasma and wall currents, as a function of generator loading and iron oxide injection rates, are shown in Fig. 9. For these results, positive values imply currents flowing in the downstream direction; negative currents flow in the upstream direction. The wall leakage currents all flow upstream, in the direction of lower elec-

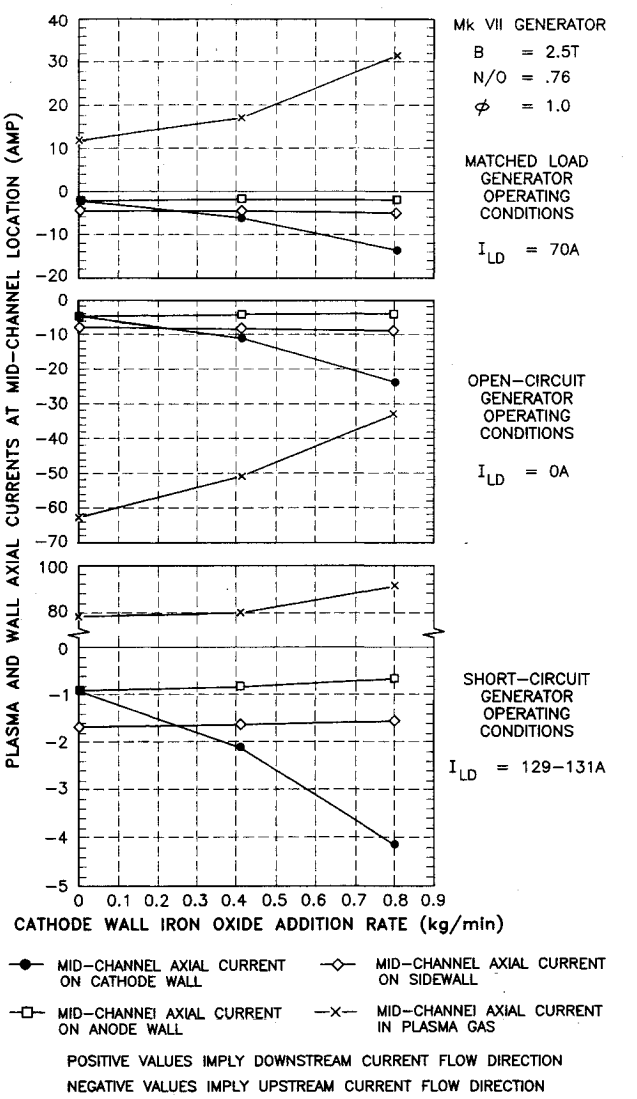

Fig. 9 Magnitudes and directions of plasma and wall axial currents at the midchannel location (X = 0.5 m).

tric potential. The returning path of the wall leakage currents is through the generator core gas region. The plasma component of the axial current becomes more positive, or less negative (depending on the generator loading), as the cathode wall leakage is increased due to increasing iron oxide addition. This plasma current, if sufficiently large, can interact with the magnetic field to produce secondary flows. This flow behavior has been suggested as a possible cause for nonuniform slag coverage observed on the anode wall of the coal-fired ITC MHD generator anode wall.[3] The effect of this axial plasma current can be neutralized somewhat by operating the generator on the open-circuit side of the matched-load condition.

Summary

An accurate account of the wall leakage currents is crucial during generator performance and data analyses. During the analysis of conductivity test data, improper accounting of the leakage currents can result in overprediction of the plasma conductivities. Also, the use of incorrect or inaccurate wall resistance distributions can lead to erroneous conclusions during generator performance analyses.

This study demonstrated that seed shutoff test data can be used to determine MHD channel wall resistance and slag layer conductivity distributions, which are then used to accurately account for internal leakage currents. The wall resistance profiles of potassium-seeded slag layers in the Mk-VII generator channels have constant σ_{slag} axial distributions. The internal wall leakages are strongly affected by iron oxide slurry injection on the cathode wall. The wall resistance profiles of iron oxide doped slag layers are unique to individual tests and specific facilities. In general, they are found to be a function of iron oxide injection rate, method of injection, and injector location.

Iron oxide addition on the cathode wall can contribute to increased axial current flow in the generator core plasma. This current, if it becomes large, can interact with the magnetic field and induce secondary flows. In the diagonally loaded MHD generator, this axial current can be neutralized somewhat by operating the generator on the open-circuit side of the matched-load condition.

Finally, the analysis showed that surface leakage effects decrease with increasing generator channel size. Axial current leakage scales directly with the local Hall field, with the wetted channel cross-sectional perimeter, and inversely with the wall resistance.

Appendix A: Determination of Plasma Conductivity

The plasma electrical conductivity in the MHD generator channel is obtained using a voltage-controlled dc power supply connected between the nozzle and the diffuser. The electrical connection during conductivity measurements is shown in Fig. 3. The electrodes of the generator are used as voltage probes to measure the axial voltage distribution within the channel. The power supply voltage settings are typically 400 V for the Mk-VII channels and 1 kV for the CDIF generator channels. The plasma conductivity σ_{plasma}, at a given location X, is determined from

$$\sigma_{plasma}(X) = \frac{L(X)I_{ps}}{A(X)\Delta V(X)} \tag{A1}$$

Appendix B: Determination of Wall Resistance and Slag Conductivity

The approaches used to estimate the values of the wall resistance and slag conductivity from the seed shutoff test data are described in this Appendix.

Equivalent Four-Wall Resistance

The axial wall resistance (at an axial location X_a) is estimated from the values of the interelectrode voltage (at X_a) and the power supply current, which are measured after the termination of the seed flow:

$$R_{gap}(X_a) = \frac{\Delta V(X_a)}{I_{ps}[L(X_a)/p]} \tag{B1}$$

Equation (B1) was used to establish the R_{gap} distributions shown in Fig. 6.

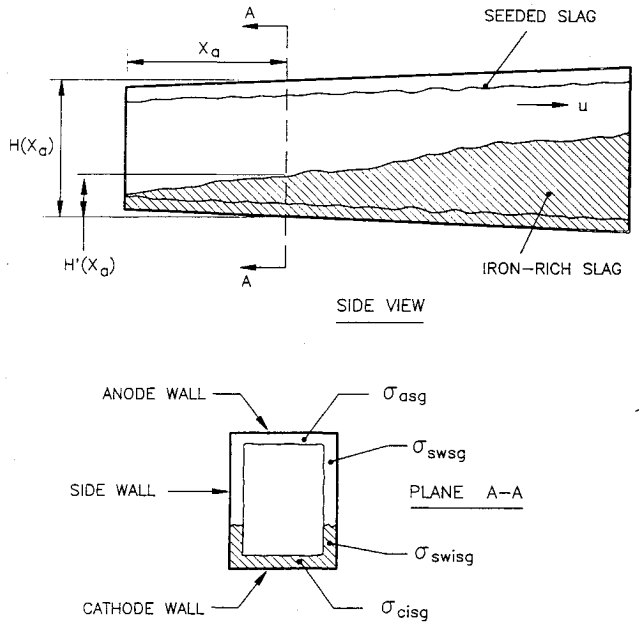

Fig. B1 Schematic diagram showing the spreading of the iron oxide wake in an MHD generator channel.

Electrical Conductivity of Potassium-Seeded Slag Layers

The values of the slag layer electrical conductivity can be inferred from the measured R_{gap}. In the absence of iron oxide addition the definition of $R_{gap}(X_a)$ is

$$R_{gap}(X_a) = p/\{s[2\sigma_{swsg}(X_a)H(X_a) + \sigma_{asg}(X_a)W(X_a) + \sigma_{csg}(X_a)W(X_a)]\} \tag{B2}$$

For simplicity, one can assume in Eq. (B2) that, at any axial location, the slag conductivity is approximately the same for the top, bottom, and side walls (i.e., the slag conductivity varies only with streamwise location). The value of the slag layer electrical conductivity σ_{slag} at location X_a can then be estimated from

$$R_{gap}(X_a) = p/[\sigma_{slag}(X_a)sP(X_a)] \tag{B3}$$

The value of R_{gap} is determined from measured data and Eq. (B1). This method was used to estimate the values of potassium-seeded slag layer electrical conductivity (without iron oxide injection) shown in Fig. 7.

Electrical Conductivity of Iron-Rich Slag Layers

In the Mk-VII MHD generator tests, the iron oxide slurry is injected onto the cathode wall through injector ports situated in the flow nozzle upstream of the channel inlet. The resulting iron oxide wake spreads along the cathode wall and up the two sidewalls, as shown in the sketch of Fig. B1. The definition of $R_{gap}(X_a)$ from Eq. (B2) is

$$R_{gap}(X_a) = p/\{2s\sigma_{swsg}(X_a)[H(X_a) - H'(X_a)] + \sigma_{asg}(X_a)sW(X_a) + 2s\sigma_{swisg}(X_a)H'(X_a) + \sigma_{cisg}(X_a)sW(X_a)\} \tag{B4}$$

Notations for the various slag layer regions are shown in Fig. B1. Assuming

$$\sigma_{swisg}(X_a) = \sigma_{cisg}(X_a) = \sigma_{isg}(X_a)$$

$$\sigma_{swsg}(X_a) = \sigma_{asg}(X_a) = \sigma_{sg}(X_a)$$

Eq. (B4) reduces to

$$R_{gap}(X_a) = p/(s\{\sigma_{sg}(X_a)[2H(X_a) - 2H'(X_a) + W(X_a)] + \sigma_{isg}(X_a)[2H'(X_a) + W(X_a)]\}) \quad \text{(B5)}$$

The value of slag layer conductivity for any wall surface with iron oxide present (σ_{isg}) can be deduced from Eq. (B5) at any axial location along the channel. To do this one must know five things: 1) the value of the measured four-wall equivalent R_{gap} during iron oxide injection (determined during seed shutoff tests); 2) the geometry of the channel; 3) the slag layer thickness (typically 1 to 2 mm); 4) the conductivity of slag with no iron oxide [σ_{sg}, ascertained during seed shutoff with no iron oxide addition and from Eq. (B3)]; and 5) the height of the iron oxide wake H'. The value of H' is based on the observed patterns of the iron oxide wakes during posttest inspection of the channel walls.

Acknowledgment

This work was sponsored by the U.S. Department of Energy and funded through Mountain States Energy, Inc., under subcontract 93-C185-CR.

References

[1]Petty, S. W., "Effects of Cathode Slag Polarization on MHD Generator Performance," *Proceedings of the 21st Symposium on the Engineering Aspects of MHD*, Argonne National Lab., Argonne, IL, 1983, pp. 4.5.1–4.5.12.

[2]McClaine, A. W., Pian, C. C. P., Petty, S. W., Pakko, J. D., and Schmitt, E. W., "Strategies for Combating Problems Caused by Cathode Slag Shorting," *Proceedings of the 26th Symposium on the Engineering Aspects of MHD*, Univ. of Tennessee Space Inst., Tullahoma, TN, 1988, pp. 3.4.1–3.4.9.

[3]Pian, C. C. P., and Schmitt, E. W., "Wall Surface Leakage Effects on MHD Power Generator Performance," Textron Defense Systems, Inc., Final Rept. to Mountain States Energy, Inc., Contract 93-C185-CR, March 1994; also *Proceedings of the 32nd Symposium on the Engineering Aspects of MHD*, DOE's Pittsburgh Energy Technology Center, Pittsburgh, PA, 1994.

[4]McClaine, A. W., "Analysis of CDIF Data from Sept. 29 1982 Experiment, Summary of the Channel Design Power Test (July–Oct. 1982)," Mountain States Energy, Appendix B, Rept. 2DOE-MHD-D104, Sept. 1982.

[5]Nelson, G. L., Lee, M. Y., Stepan, I., Lineberry, J. T., and Wu, Y. C. L., "Analysis of CDIF Coal-Fired Faraday Generator Test Data," *Proceedings of the 27th Symposium on the Engineering Aspects of MHD* (Reno, NV), TRW, Applied Technology Div., Redondo Beach, CA, 1989, pp. 4.3.1–4.3.16.

[6]Lineberry, J. T., Wu, Y. C. L., and Daniel, V. W., "An Assessment of Factors Affecting Generator Performance Based on Recent Results of CDIF Data Studies," *Proceedings of the 30th Symposium on the Engineering Aspects of MHD* (Baltimore, MD), Gilbert/Commonwealth, Inc., Reading, PA, 1992 (Paper IX.1).

[7]"MHD Channel Development," Avco Research Lab., Rept. DOE/ET-70507-12, April 1987, pp. 75–91.

[8]Rosa, R. J., "Leakage Resistance and Current Inferred from CDIF Operating Data," *Proceedings of the 28th Symposium on the Engineering Aspects of MHD* (Chicago, IL), Argonne National Lab., Argonne, IL, 1990 (Paper VI.4).

[9]Daniel, V. W., "Estimating Plasma/Slag Properties from CDIF Electrical Measurements," AIAA Paper 91-1515, June 1991.

[10]Pian, C. C. P., Schmitt, E. W., Farrar, L. C., and Petty, S. W., "Generator Performance Experiments Supporting the Prototypic MHD Channel Design," *Proceedings of the 28th Symposium on the Engineering Aspects of MHD* (Chicago, IL), Argonne National Lab., Argonne, IL, 1990 (Paper VI.1).

[11]Pian, C. C. P., "Data Analysis of Diagonally-Connected MHD Power Generator Experiments," AIAA Paper 86-0129, Jan. 1986.

[12]Pian, C. C. P., and McClaine, A. W., "Techniques for the Solution of MHD Generator Flows," *Computers and Fluids*, Vol. 12, No. 4, 1984, pp. 319–338.